Photodetector without Electron Transport Layer Based on Hexane-1,6-Diammonium Pentaiodobismuth (HDA-BiI$_5$) Molecular Semiconductor

Yifei Wang, Xiaoping Zou *, Jialin Zhu *, Chunqian Zhang, Jin Cheng, Junqi Wang, Xiaolan Wang, Xiaotong Li, Keke Song, Baokai Ren and Junming Li

Beijing Advanced Innovation Center for Materials Genome Engineering, Research Center for Sensor Technology, Beijing Key Laboratory for Sensor, Beijing Key Laboratory for Optoelectronic Measurement Technology, MOE Key Laboratory for Modern Measurement and Control Technology, School of Automation, Beijing Information Science and Technology University, Jianxiangqiao Campus, Beijing 100101, China; yifeiwang2020@126.com (Y.W.); chunqiancool@163.com (C.Z.); chengjin@bistu.edu.cn (J.C.); 13126706081@163.com (J.W.); wangxl1105@163.com (X.W.); xiaotong252240@163.com (X.L.); songmengke163@163.com (K.S.); renbk2021@163.com (B.R.); li@physik.HU-berlin.de (J.L.)
* Correspondence: xpzou2021@163.com (X.Z.); jlzhu@bistu.edu.cn (J.Z.)

Abstract: With the development of the semiconductor industry, research on photoelectronic devices has been emphasized. In this paper, a molecular semiconductor material with a narrow bandgap of hexane-1,6-diammonium pentaiodobismuth (HDA-BiI$_5$) was utilized to prepare photodetectors without electron transport layers. Using a single light source, the effects of different wavelengths and different powers on the photoresponsivity, switching ratio, specific detectivity, and external quantum efficiency of the device were investigated. It is demonstrated that this device has excellent responsivity, specific detectivity, stability, and repeatability, and this work will help expand the application of molecular semiconductor materials for photodetection.

Keywords: photodetector; molecular semiconductor; thin films

1. Introduction

In recent years, with the wide application of photodetectors in medical, sensing, and communication industries [1–6], various types of photodetectors are emerging. For example, Mehbuba Tanzid, et al. combined hot carrier-based photodetection with free carrier absorption (FCA) in highly doped p-type silicon to create a narrow-band NIR photodetector structure with enhanced performance, obtaining high responsivity with minimal noise equivalent, respectively, at relatively low bias [7]. Ibrahima Ka et al. reported the use of a pulsed laser deposition (PLD) technique to decorate double-walled carbon nanotubes (DWCNTs) with PbS quantum dots (QDs) to form a new class of physically synthesized nanohybrid (NH) materials. The nanohybrid materials were applied to photodetectors and the devices obtained high performance [8]. The use of novel technologies can enhance a detector's performance, but it is also important to find suitable materials and device structures [9–13]. For devices, both material and device structure are two of the main factors affecting the performance [14,15]. Yet, few people have studied the photoelectric performance of molecular semiconductor materials without an electron transport layer. According to previous reports, a new molecular semiconductor material hexane-1, 6-diammonium pentaiodobismuth (HDA-BiI$_5$), with the narrowest bandgap (~1.89 eV) [16] and a wide range of light absorption, has a bright prospect for future applications in photoelectric detection [17–19]. David M. Fabian et al. prepared solar cells with conventional structures using HDA-BiI$_5$ as a light-absorbing layer on FTO substrates and found good stability after testing [20]. However, the effect on the performance was not further investigated by changing the device structure, we made photodetectors without

electron transport layer to study. In addition, Liu et al. used the molecular semiconductor material HDA-BiI$_5$ to prepare conventional structured solar devices and tested the relevant photovoltaic performance under solar light conditions [21]. It is not enough to characterize performance only under solar light conditions. HDA-BiI$_5$ has a narrow bandgap with a wide range of light absorption, so we investigated the performance of the devices by varying the incident light at different wavelengths and powers under single light source.

Here, we prepare photodetectors with ITO/NiO$_x$/HDA-BiI$_5$/Al structure without electron transport layer on ITO substrate using HDA-BiI$_5$ molecular semiconductor material as the light-absorbing layer and test the photoelectric performance of the devices using a single light source. The effects of different powers at 532 and 375 nm wavelengths laser on the photoresponsivity, switching ratio, specific detection rate, and external quantum efficiency were also investigated. It was found that this device has good photoresponsivity and specific detectivity, which provides a basis for the future use of molecular semiconductor materials as a light-absorbing layer in the study of photodetection of different structures, thus further expanding the application of molecular semiconductor materials.

2. Experimental

2.1. Materials

The conductive substrate used in this paper is a conductive glass containing indium tin oxide (ITO), from South China Xiangcheng Technology Co., Shenzhen, China. The thickness is about 1.1 mm, the square resistance is $\leq$5 Ω, and the transmittance is $\geq$84%. The concentration of high temperature nickel oxide spin coating solution (HT-NiO$_x$) used in the experiments was 0.5 M, which was obtained from Shanghai Maituowei Technology Co., Shanghai, China. N,N-Dimethylformamide (DMF) with a purity of 99.8% was used from Alfa Aesar (Shanghai, China) Chemical Co. The experiments were conducted using HI with a purity of 45% and BiI$_3$ with a purity of 99.99%, which were obtained from Shanghai Maikelin Biochemical Technology Co. (Shanghai, China) and Shanghai Aladdin Biochemical Technology Co. (Shanghai, China). 1,6-diaminohexane with purity of AR was purchased from Sinopharm Chemical Reagent Co. (Beijing, China). Other materials are commonly used in laboratory.

2.2. Device Fabrication

Details of HDA-BiI$_5$ crystal synthesis, cleaning ITO conductive glass, characterization, and photoelectronic test platform are in the supporting information.

(1) Preparation of hole transport layer

In this experiment, a high-temperature nickel oxide spin-coating solution was chosen for the preparation of the hole transport layer. During the preparation of the NiO$_x$ hole transport layer, 40 μL of HT-NiO$_x$ spin-coating solution was first applied to the ITO conductive glass substrate with a pipette, and then spin coated on ITO at 4000 rpm for 30 s. Then immediately annealed on a hot plate at 100 °C for 10 min. After annealing, sintering is carried out in a muffle furnace (Beijing Jinyang Wanda Technology Co., Beijing, China) with a sintering temperature of 300 °C, a ramp-up time of 30 min, and a constant temperature stage of 60 min.

(2) Preparation of light-absorbing layer

500 mg of HDA-BiI$_5$ powder was weighed and dissolved in 0.4 mL of DMF solution, and the solution was heated and stirred for 4 h until the powder was completely dissolved, at which time the solution turned dark brown. Next, the completely dissolved solution was filtered through a syringe with a 0.22 μm diameter filter tip to remove the residual particles that were not completely dissolved in the solution, and the HDA-BiI$_5$ solution for the preparation of the film was obtained. 40 μL of HDA-BiI$_5$ solution was spun at 6000 rpm. for 40 s using a pipette. Immediately after spin-coating, the samples were annealed on a hot plate at 150 °C for 30 min.

(3) Preparation of electrodes

In order to prepare a vertically structured photoelectric device, a gap of about 3 mm should be left at the edge of the conductive side of the ITO substrate before preparing the counter electrode, and the material prepared above should be cleaned up, so that this part of the electrode can be prepared on the ITO conductive glass substrate to form a vertically structured device. In this experiment, aluminum was chosen as the metal counter electrode and prepared by vacuum vapor deposition apparatus.

3. Results and Discussion

We characterized the HDA-BiI$_5$ films prepared on ITO. As shown in Figures S1 and S2 and Table S1, where the atomic percentages of Bi and I elements are 5.55% and 25.44%, respectively, which are consistent with the elemental molecular ratio of the molecular semiconductor material HDA-BiI$_5$. We marked some crystallographic indices of HDA-BiI$_5$, (110), (111), (120), etc. This substance belongs to the orthogonal crystal system with the point group structure of Pna2$_1$, a = 15.10390 Å, b = 14.12063 Å, c = 8.68198 Å and cell volume of 1851.6638 Å^3, all the Bragg diffraction peaks of HDA-BiI$_5$ films corresponded to the literature [16,20]. Then, we prepared the HDA-BiI$_5$ film on NiO$_x$ hole transport layer, and it can be seen in Figure 1 that the film surface is flat, however, there are a few cracks and holes. Furthermore, the film thickness reaches 1 μm, and the thickness is also a key factor affecting device performance, an appropriately thick light-absorbing layer can improve the photovoltaic performance, which can be attributed to the increased light absorption and light collection efficiency [21–23]. In addition, it is known from previous studies that HDA-BiI$_5$ is an N-type material [20]. This promotes the transport of photogenerated carriers inside the layers at the PN junction. The occurrence of electron-hole recombination is avoided, reducing the occurrence of short circuits. For device performance, it is also important to have good light absorption capability. From Figure 2c, demonstrates that the wavelength range of the absorbed light is 400–660 nm, and the absorption edge is about 645 nm, indicating a bandgap of about 1.92 eV. The relative positions of the conduction and valence bands of HDA-BiI$_5$ were measured using ultraviolet photoemission spectra (UPS), as shown in Figure S3 (Supporting Information). E$_f$ was 5.01 eV and E$_{Cutoff}$ was 16.21 eV. Using the optical band gap (1.92 eV), E$_f$, E$_{Cutoff}$, and excitation energy (21.22 eV), the valence band maximum (VBM) of HDA-BiI5 was calculated to be 6.58 eV at 1.57 eV below E$_f$, and the conduction band maximum (CBM) was 4.66 eV.

After the device was prepared as the structure of Figure 2a, we performed the photoelectric performance test. The photoresponse characteristics curve of the photodetector without an electron transport layer under zero-bias 375 nm laser with a switching time of 1 s is shown in Figure 3a. This device can rapidly generate repeatable photocurrents when irradiated by a 375 nm laser, which is caused by the increase in the carrier mobility in a short period time. At the same light power, the photocurrent does not change much with the change of switching time, which means that this device has reached the maximum photocurrent in 1 s. Moreover, the device responds quickly at different light power, whether light-on and light-off. When the photocurrent reaches a maximum value, it then gradually decreases to a steady-state value probably due to the sudden separation of photogenerated carriers after being exposed to light. After a period of time, the current gradually decreases and finally achieves a steady-state photocurrent due to the balance between the diffusion rate of carriers and their generation rate. We performed 10 consecutive switching operations, and it can be seen that the photocurrent remained basically unchanged. The response time curve of HDA-BiI$_5$ based on a photoelectric device under laser irradiation at 375 nm, 4.74 mW power is shown in Figure 3b. When the laser is turned off, the sharp drop of the photocurrent to the dark current is observed, which can reflect the capacitive response of the surface state of the light-absorbing layer. In addition, we take 10–90% of the response as rise time and 90–10% as decay time. It can be seen that the device rise time is about 61 ms and decay time is about 62 ms. This indicates that the device can rapidly generate photocurrents with a repeatable response and demonstrates the stability of the device under frequent switching.
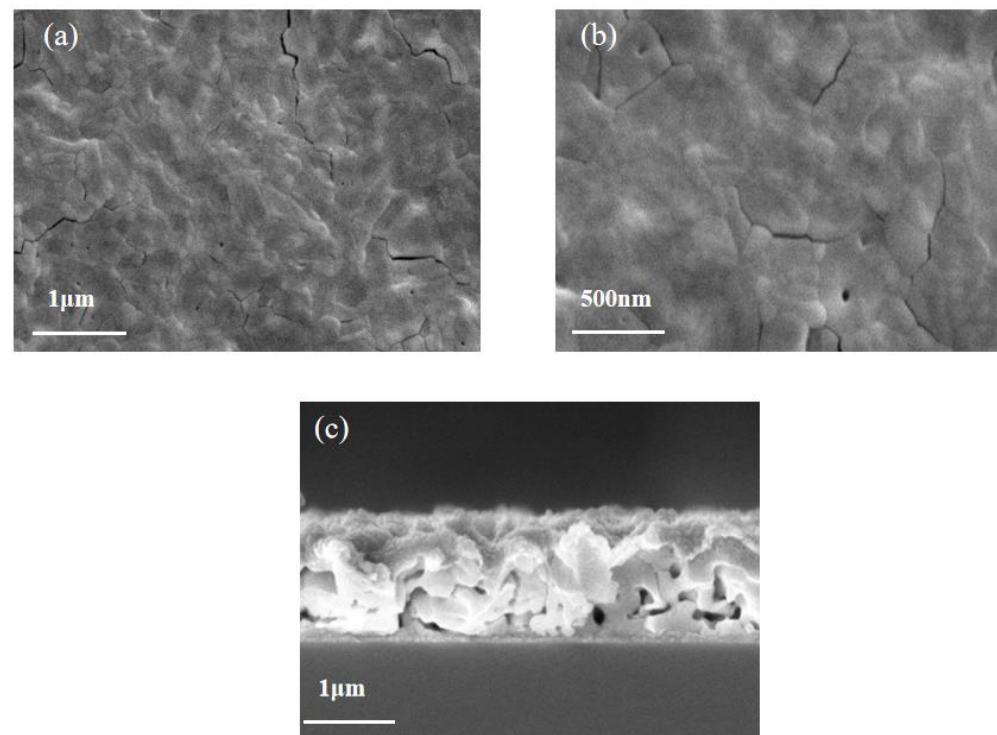
Figure 1. SEM images of HDA-BiI$_5$ layer (**a**) top view, (**b**) enlarged view, (**c**) cross-sectional view.
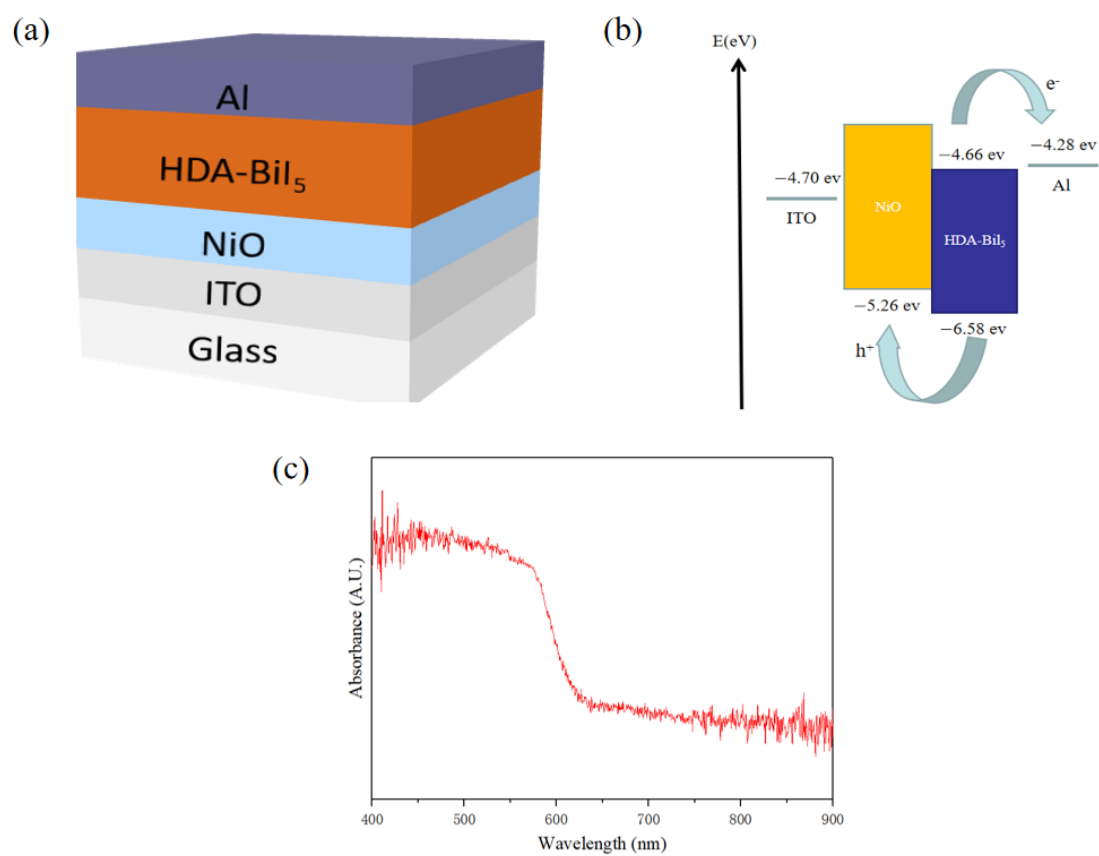

Figure 2. (**a**) Schematic diagram of the structure, (**b**) Energy band structure of each material in the ITO/NiO$_x$/HDA-BiI$_5$/Al device. (**c**) UV-vis absorption spectra.

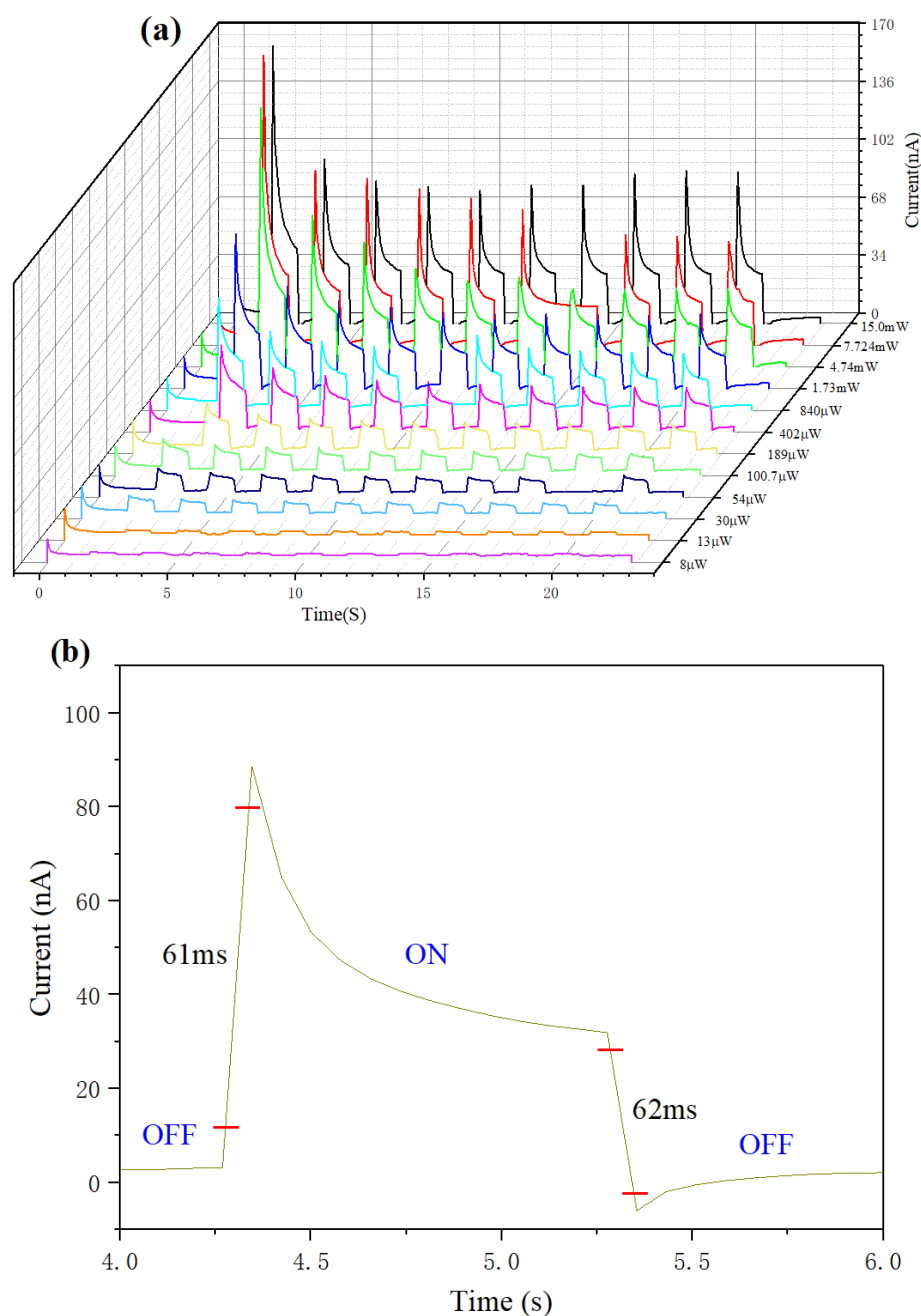**Figure 3.** (**a**) Photoresponse characteristics under zero-bias 375 nm laser. (**b**) Response time of HDA-BiI$_5$-based photoelectronic devices at the wavelength of 375 nm and a power of 4.74 mW.

It is well known that photodetectors are converted from optical signals to electrical signals. The electrons in the valence band are excited into the conduction band after absorbing the energy of the incident photons, and thus produce a free moving electron in the conduction band and leaving a hole in the valence band. Then, the electron and hole are transferred to the electrode, as shown in Figure 1b. In order to further verify the other performance indexes of the photodetector, experiment using the short-wave light irradiation of 375 nm. Fitting photoresponse characteristics of HDA-BiI$_5$-based photodetectors under 375 nm laser are shown in Figure 4, it was found that the photoresponsivity of the device can reach 5.37×10^{-4} A/W and the specific detectivity can reach 5.9×10^{10} Jones. The short-wave light has a larger energy which can excite more electrons from the valence band into the conduction band and thus achieve a greater contribution to the photocurrent [24]. This suggests that photoionization will be further enhanced with one carrier

being trapped and another carrier flowing in a circular fashion, which reduces the large recombination of electron-hole pairs, enhancing photodetector performance [25]. The performance of this device is attractive compared to other similar detectors, and a comparison chart of the performance parameters with other similar devices is presented in Table 1 [20,21,26–33]. According to previous literature reports, the HDA-BiI$_5$-based device study did not systematically analyze the relevant parameter performance of the detector [20,21], however, compared with detectors of other materials, although some devices exhibit lower dark currents, our device is still very competitive as a photodetector without electron transport layer structure, considering the overall photoelectronic performance and simple fabrication process.

Table 1. Comparison of HDA-BiI$_5$- based photodetector with other similarly structured materials devices.

Photodetector	ETL (Yes/No)	Polarization (Yes/No)	Light (nm)	Dark Current (pA)	Responsivity (A/W)	Detectivity [Jones]	Rise and Decay Time (s)	Ref.
BaTiO$_3$	No	No	365	-	3.48×10^{-9}	2.06×10^4	-	[26]
PLZT8	No	No	405	>22	4.48×10^{-7}	7.15×10^7	-	[27]
BaTiO$_3$	No	No	405	>100	$<3.5 \times 10^{-7}$	$<3.5 \times 10^5$	0.4/1.6	[28]
BiFeO$_3$	No	Yes	450	>100	$\sim 10^{-7}$	$\sim 10^8$	0.5/0.8	[29]
PLZT	No	Yes	375	3	$<5 \times 10^{-5}$	$<9.52 \times 10^8$	>0.42/0.46	[30]
	No	Yes	532		$<2.5 \times 10^{-5}$	$<9.52 \times 10^8$	>0.42/0.46	
	No	Yes	375	2	$<1 \times 10^{-4}$	$<3.69 \times 10^9$	0.34/0.36	
	No	Yes	532		$<2.5 \times 10^{-5}$	$<3.69 \times 10^9$	>0.34/0.36	
BaTiO$_3$	No	No	405	-	$\sim 10^{-7}$	10^5	0.6/0.5	[31]
BaTiO$_3$	No	No	365	-	$\sim 10^{-7}$	—	0.56/13.44	[32]
TiO$_2$:P3HT	Yes	No	375	>103	$<5 \times 10^{-4}$	$<10^{-8}$	>0.52/0.87	[33]
	Yes	No	532		$<4.5 \times 10^{-4}$	$<10^{-8}$	>0.52/0.87	
HDA-BiI$_5$	Yes	Yes	sunlight illumination	-	-	-	-	[21]
HDA-BiI$_5$	Yes	No	sunlight illumination	-	-	-	-	[20]
HDA-BiI$_5$	No	No	375	16	5.37×10^{-4}	5.9×10^{10}	0.061/0.062	This work
	No	No	532		1.28×10^{-4}	1.4×10^{10}	0.062/0.063	

To further investigate the effect of wavelengths of laser on the photoelectric performance of the detector, we use 532 nm wavelength laser for the photoelectric performance test. The photoresponse characteristics curve of the photodetector without electron transport layer under zero-bias 532 nm laser with a switching time of 1 s is shown in Figure 5a. At the same light power, the photocurrent basically does not vary with the switching time, and there is a very low dark current which contributes significantly to the device stability. The response time curve of HDA-BiI$_5$-based photodetectors under laser irradiation at 532 nm, 49.4 mW power is shown in Figure 5b. We take 10–90% of the response as rise time and 90–10% as decay time. It can be seen that the device rise time is about 62 ms and decay time is about 63 ms. However, the value of the photocurrent decreases compared to the 375 nm laser irradiation, and it can be seen from Figure 5b that the response is slower in the no-light-to-light process. This may be related to the transport speed and transport efficiency of electrons and holes in the PN junction, which eventually leads to a longer rising time from no light to light in the photoelectric device.
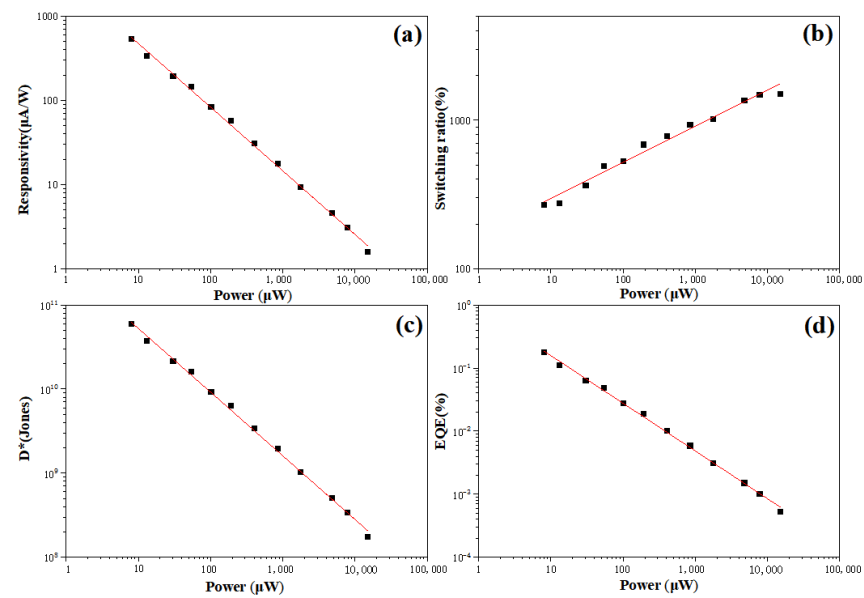
Figure 4. Fitting photoresponse characteristics of HDA-BiI$_5$-based photodetectors under 375 nm laser: (**a**) photoresponsivity, (**b**) switching ratio, (**c**) specific detectivity, (**d**) External quantum efficiency.
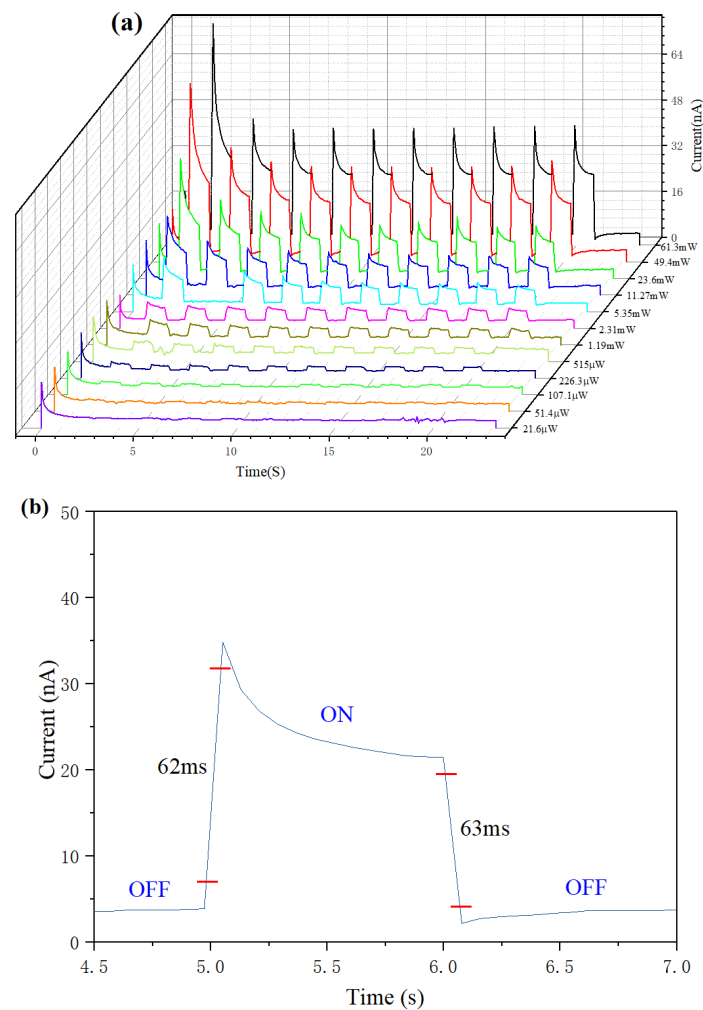

Figure 5. (**a**) Photoresponse characteristics under zero-bias 532 nm laser. (**b**) Response time of HDA-BiI$_5$-based photoelectric devices at the wavelength of 532 nm and a power of 49.4 mW.

As can be seen in Figure 6, the photoresponsivity increases rapidly with decreasing light power, and importantly, a high photoresponsivity of 130 μA/W is observed even at very low light power, which indicates that our photodetector provides low power consumption characteristics. With increasing photopower, the photocurrent has a dependence on it. The decrease in photoresponsivity can be explained by the presence of trap states at the interface between HDA-BiI$_5$ and NiO$_x$ and the attachment of charged impurities or molecules on the HDA-BiI$_5$ film [34]. Under the illumination of high light power, the density of available states decreases and photoinduced carriers can fill more traps, leading to saturation of the photoresponse [35,36]. In addition, probably due to the effect of upper layer oxidation, Al electrodes are easily oxidized in air, and the presence of a thin oxide (Al$_2$O$_3$) layer around the electrode makes the thickness of the Al electrode increase, which can lead to a substantial attenuation of the tunneling current and subsequent reduction in photon yield, affecting the density of states in the carrier local mode. This effect is the reduction of electron motion or tunneling when passing through the potential barrier, avoiding the excitation of the dynamic plasma mode, thus affecting the photodetection performance of the photodetector [37]. As the incident light power increases, the bright-to-dark current ratio, specific detectivity and quantum efficiency follow a similar trend to the curves in Figure 4. However, the performance under 532 nm laser irradiation is all degraded compared to that under 375 nm laser irradiation. This is mainly because as the laser wavelength increases, the photon energy becomes smaller, and the electron-hole pairs produced by light are mainly excited by light with energy greater than the HDA-BiI$_5$ bandgap [38]. Fewer electron-hole pairs are excited, and part of the electron-hole fills the trap and the other part is transferred to the electrode, resulting in reduced values of photoresponsivity, switching ratio, specific detection rate, and quantum efficiency compared to those at 375 nm.
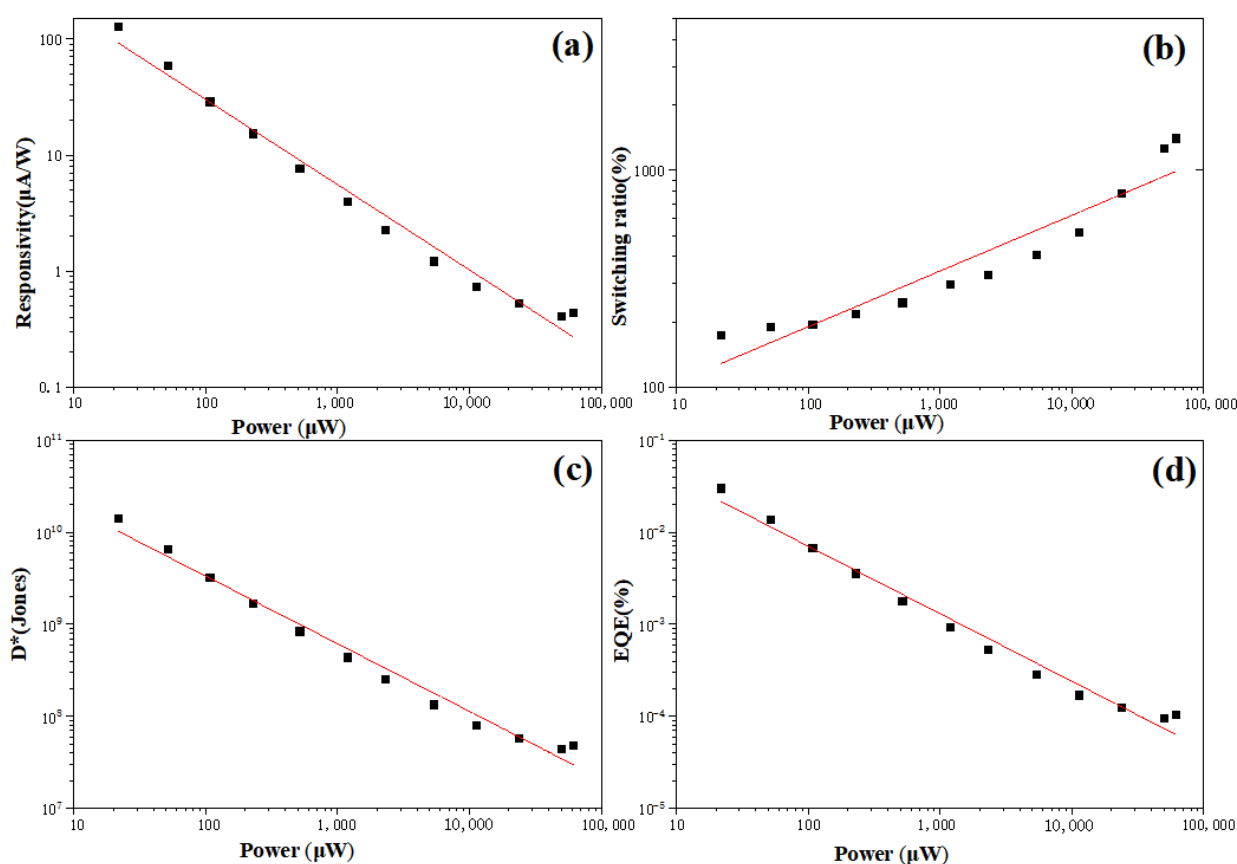

Figure 6. Fitting photoresponse characteristics of HDA-BiI$_5$-based photodetectors under 532 nm laser: (**a**) photoresponsivity, (**b**) switching ratio, (**c**) specific detectivity, (**d**) External quantum efficiency.

4. Conclusions

The molecular semiconductor material HDA-BiI$_5$ was used to prepare the photodetector without ETL, and the photoelectric performance of the structure device was tested under a single light source at 532 and 375 nm, respectively. We found that the device has a fast response time and has a high photoresponsivity and specific detection rate at low light power which provides low power consumption characteristics for the detector. In addition, the photodetector showed good stability and repeatability during 10 times of light-on and light-off. The effect on the device performance at different power levels is investigated, which provides some information for future research on molecular semiconductor materials to prepare inverted structure devices. In response to the above results, the photodetector can be extended for applications in communication, tracking technology, space detection, etc., which provides a bright future for future research on photodetectors.

Supplementary Materials: The following are available online at https://www.mdpi.com/article/10.3390/coatings11091099/s1, Figure S1: XRD pattern of HDA-BiI$_5$ film on ITO, Figure S2: EDS results of analyzed, Table S1: The types and percentages of some elements obtained from EDS analysis, Figure S3. Ultraviolet photoemission spectra (He I) of HDABiI5/ITO.

References

1. Baeg, K.J.; Binda, M.; Natali, D.; Caironi, M.; Noh, Y.Y. Organic light detectors: Photodiodes and phototransistors. *Adv. Mater.* **2013**, *25*, 4267–4295. [CrossRef] [PubMed]
2. Li, G.; Gang, W.; Shi, M.; Yang, G.; Chen, Z.; Wang, M. ZnO/poly(9,9-dihexylfluorene) based inorganic/organic hybrid ultraviolet photodetector. *Appl. Phys. Lett.* **2008**, *93*, 383. [CrossRef]
3. Mazzillo, M.; Condorelli, G.; Castagna, M.E.; Catania, G.; Sciuto, A.; Roccaforte, F.; Raineri, V. Highly efficient low reverse biased 4H-SiC schottky photodiodes for UV-light detection. *IEEE Photon. Technol. Lett.* **2009**, *21*, 1782–1784. [CrossRef]
4. Wang, L.; Zhao, D.; Su, Z.; Fang, F.; Li, B.; Zhang, Z.; Shen, D.; Wang, X. High spectrum selectivity organic/inorganic hybrid visible-blind ultraviolet photodetector based on ZnO nanorods. *Organic Electron. Phys. Mater. Appl.* **2010**, *11*, 1318–1322. [CrossRef]
5. Gong, X.; Tong, M.; Xia, Y.; Cai, W.; Moon, J.S.; Cao, Y.; Yu, G.; Shieh, C.-L.; Nilsson, B.; Heeger, A.J. High-detectivity polymer photodetectors with spectral response from 300 nm to 1450 nm. *Science* **2009**, *325*, 1665–1667. [CrossRef] [PubMed]
6. Zhu, L.; Dai, Q.; Hu, Z.-F.; Zhang, X.-Q.; Wang, Y.-S. Organic deep ultraviolet photodetector with response peak focusing on 270 nm using the acceptor BAlq. *IEEE Photon.-Technol. Lett.* **2011**, *23*, 1835–1837. [CrossRef]
7. Tanzid, M.; Ahmadivand, A.; Zhang, R.M.; Cerjan, B.; Sobhani, A.; Yazdi, S.; Nordlander, P.; Halas, N.J. Combining plasmonic hot carrier generation with free carrier absorption for high-performance near-infrared silicon-based photodetection. *ACS Photon.* **2018**, *5*, 3472–3477. [CrossRef]
8. Ka, I.; Le Borgne, V.; Fujisawa, K.; Hayashi, T.; Kim, Y.A.; Endo, M.; Ma, D.L.; El Khakani, M.A. PbS-quantum-dots/double-wall-carbon-nanotubes nanohybrid based photodetectors with extremely fast response and high responsivity. *Mater. Today Energy* **2020**, *16*, 9. [CrossRef]
9. Arredondo, B.; de Dios, C.; Vergaz, R.; Criado, A.; Romero, B.; Zimmermann, B.; Würfel, U. Performance of ITO-free inverted organic bulk heterojunction photodetectors: Comparison with standard device architecture. *Org. Electron.* **2013**, *14*, 2484–2490. [CrossRef]
10. Chang, Y.-M.; Leu, C.-Y. Conjugated polyelectrolyte and zinc oxide stacked structure as an interlayer in highly efficient and stable organic photovoltaic cells. *J. Mater. Chem. A* **2013**, *1*, 6446–6451. [CrossRef]

11. Hau, S.K.; Yip, H.L.; Hong, M.; Jen, K.Y. High performance ambient processed inverted polymer solar cells through interfacial modification with a fullerene self-assembled monolayer. *Appl. Phys. Lett.* **2008**, *93*, 441. [CrossRef]

12. Sun, Y.; Seo, J.H.; Takacs, C.J.; Seifter, J.; Heeger, A.J. Inverted polymer solar cells integrated with a low-temperature-annealed sol-gel-derived ZnO film as an electron transport layer. *Adv. Mater.* **2011**, *23*, 1679–1683. [CrossRef] [PubMed]

13. Yang, T.; Cai, W.; Qin, D.; Wang, E.; Lan, L.; Gong, X.; Peng, J.; Cao, Y. Solution-processed zinc oxide thin film as a buffer layer for polymer solar cells with an inverted device structure. *J. Phys. Chem. C* **2010**, *114*, 6849–6853. [CrossRef]

14. Upadhyay, D.C.; Upadhyay, R.K.; Singh, A.P.; Jit, S. High-performance inverted structure broadband photodetector based on ZnO nanorods/PCDTBT:PCBM:PbS QDs. *IEEE Trans. Electron Dev.* **2020**, *67*, 4970–4976. [CrossRef]

15. Wu, S.; Xiao, B.; Zhao, B.; He, Z.; Wu, H.; Cao, Y. High sensitivity polymer visible-near infrared photo-detectors via an inverted device structure and manipulation of injection barrier height. *Small* **2016**, *12*, 3374–3380. [CrossRef] [PubMed]

16. Zhang, H.-Y.; Wei, Z.; Li, P.-F.; Tang, Y.-Y.; Liao, W.-Q.; Ye, H.-Y.; Cai, H.; Xiong, R.-G. The narrowest band gap ever observed in molecular ferroelectrics: Hexane-1,6-diammonium pentaiodobismuth(III). *Angew. Chem. Int. Ed.* **2017**, *57*, 526–530. [CrossRef]

17. Guo, D.; Su, Y.; Shi, H.; Li, P.; Zhao, N.; Ye, J.; Wang, S.; Liu, A.; Chen, Z.; Li, C. Self-powered ultraviolet photodetector with super high photoresponsivity (3.05 a/w) based on the GaN/Sn:Ga$_2$O$_3$ pn junction. *ACS Nano* **2018**, *12*, 12827–12835. [CrossRef]

18. Ouyang, B.; Chang, C.; Zhao, L.D.; Wang, Z.L.; Yang, Y. Thermo-photoelectric coupled effect induced electricity in N-type SnSe:Br single crystals for enhanced self-powered photodetectors. *Nano Energy* **2019**, *66*, 104111. [CrossRef]

19. Zhao, K.; Wang, Y.; Han, L.; Wang, Y.; Luo, X.; Zhang, Z.; Yang, Y. Nanogenerator-based self-charging energy storage devices. *Nano-Micro Lett.* **2019**, *11*, 1–19. [CrossRef] [PubMed]

20. Fabian, D.M.; Ardo, S. Hybrid organic–inorganic solar cells based on bismuth iodide and 1,6-hexanediammonium dication. *J. Mater. Chem. A* **2016**, *4*, 6837–6841. [CrossRef]

21. Liu, X.; Zhang, G.; Zhu, M.; Chen, W.; Zou, Q.; Zeng, T. Polarization-enhanced photoelectric performance in a molecular ferroelectric hexane-1,6-diammonium pentaiodobismuth (HDA-BiI5)-based solar device. *RSC Adv.* **2020**, *10*, 1198–1203. [CrossRef]

22. Zhang, G.; Zhang, Q.; Hu, Q.; Wang, B.; Yang, W. Giant enhancements in electronic transport and photoelectric properties of bismuth oxysulfide by pressure-driven 2D–3D structural reconstruction. *J. Mater. Chem. A* **2019**, *7*, 4019–4025. [CrossRef]

23. He, Z.; Zhong, C.; Huang, X.; Wong, W.-Y.; Wu, H.; Chen, L.; Su, S.; Cao, Y. Simultaneous enhancement of open-circuit voltage, short-circuit current density, and fill factor in polymer solar cells. *Adv. Mater.* **2011**, *23*, 4636–4643. [CrossRef] [PubMed]

24. Hu, X.; Zhang, X.D.; Liang, L.; Bao, J.; Li, S.; Yang, W.L.; Xie, Y. High-performance flexible broadband photodetector based on organolead halide perovskite. *Adv. Funct. Mater.* **2014**, *24*, 7373–7380. [CrossRef]

25. Sukhovatkin, V.; Hinds, S.; Brzozowski, L.; Sargent, E.H. Colloidal quantum-dot photodetectors exploiting multiexciton generation. *Science* **2009**, *324*, 1542–1544. [CrossRef] [PubMed]

26. Ma, N.; Yang, Y. Enhanced self-powered UV photoresponse of ferroelectric BaTiO$_3$ materials by pyroelectric effect. *Nano Energy* **2017**, *40*, 352–359. [CrossRef]

27. Huangfu, G.; Xiao, H.; Guan, L.; Zhong, H.; Hu, C.; Shi, Z.; Guo, Y. Visible or near-infrared light self-powered photodetectors based on transparent ferroelectric ceramics. *ACS Appl. Mater. Interfaces* **2020**, *12*, 33950–33959. [CrossRef] [PubMed]

28. Ma, N.; Zhang, K.; Yang, Y. Photovoltaic–pyroelectric coupled effect induced electricity for self-powered photodetector system. *Adv. Mater.* **2017**, *29*, 10. [CrossRef]

29. Qi, J.; Ma, N.; Yang, Y. Photovoltaic-pyroelectric coupled effect based nanogenerators for self-powered photo-detector system. *Adv. Mater. Interfaces* **2018**, *5*, 8. [CrossRef]

30. Chen, J.; Priya, A.S.; You, D.; Pei, W.; Zhang, Q.; Lu, Y.; Li, M.; Guo, J.; He, Y. Self-driven ultraviolet photodetectors based on ferroelectric depolarization field and interfacial potential. *Sens. Actuators A Phys.* **2020**, *315*, 112267. [CrossRef]

31. Ma, N.; Yang, Y. Boosted photocurrent in ferroelectric BaTiO$_3$ materials via two dimensional planar-structured contact configurations. *Nano Energy* **2018**, *50*, 417–424. [CrossRef]

32. Song, K.; Ma, N.; Mishra, Y.; Adelung, R.; Yang, Y. Achieving light-induced ultrahigh pyroelectric charge density toward self-powered UV light detection. *Adv. Electron. Mater.* **2019**, *5*, 8. [CrossRef]

33. Shen, T.; Chu, Y.; Liao, Y.; Lee, W.; Kuo, H.; Lin, T.; Chen, Y. Ultrahigh-performance self-powered flexible photodetector driven from photogating, piezo-phototronic, and ferroelectric effects. *Adv. Opt. Mater.* **2020**, *8*, 8. [CrossRef]

34. Ghatak, S.; Pal, A.N.; Ghosh, A. Nature of electronic states in atomically thin MoS$_2$ field-effect transistors. *ACS Nano* **2011**, *5*, 7707–7712. [CrossRef] [PubMed]

35. Lopez-Sanchez, O.; Lembke, D.; Kayci, M.; Radenovic, A.; Kis, A. Ultrasensitive photodetectors based on monolayer MoS$_2$. *Nat. Nanotechnol.* **2013**, *8*, 497–501. [CrossRef]

36. Tamalampudi, S.; Lu, Y.-Y.; U., R.K.; Sankar, R.; Liao, C.-D.; B., K.M.; Cheng, C.-H.; Chou, F.-C.; Chen, Y.-T. High performance and bendable few-layered InSe photodetectors with broad spectral response. *Nano Lett.* **2014**, *14*, 2800–2806. [CrossRef] [PubMed]

37. Ahmadivand, A. Electrically excited plasmonic ultraviolet light sources. *Small* **2021**, *17*, 2100819. [CrossRef] [PubMed]

38. Chen, X.; Liu, K.; Zhang, Z.; Wang, C.; Li, B.; Zhao, H.; Zhao, D.; Shen, D. Self-powered solar-blind photodetector with fast response based on Au/β-Ga$_2$O$_3$ nanowires array film schottky junction. *ACS Appl. Mater. Interfaces* **2016**, *8*, 4185–4191. [CrossRef] [PubMed]